

A Discontinuous Galerkin Multiscale Method for First Order Hyperbolic Equations

Mats G. Larson* Axel Målqvist[†] Robert Söderlund[‡]

January 31, 2012

Abstract

Over the last fifteen years several numerical methods have been proposed for solving partial differential equations with rapidly varying coefficients, see e.g. [6, 8]. Typical applications for such methods include oil reservoir simulation and CO₂ sequestration. In [14] an adaptive multiscale method for elliptic problems was proposed, where the adaptivity is governed by an a posteriori error estimate. These ideas were later extended to also cover the convection dominated case in [11].

In the present paper we adopt the framework presented in [14], using discontinuous Galerkin basis functions, and we apply the method to a hyperbolic model problem with applications e.g. in two phase flow in an oil reservoir. We present very promising numerical results showing that small directed patches can be used to accurately compute the local fine scale solutions which are then used to form a modified coarse scale equation.

1 Introduction

Multiscale problems appear in many applications in the engineering sciences, for instance, composite materials, porous media flow, and fluid mechanics. A common feature of multiscale problems is that they are very computationally challenging and often impossible to solve to an acceptable tolerance, with standard methods, on a single mesh.

*Professor, Department of Mathematics, Umeå University, S-901-87 Umeå, Sweden, mats.larson@math.umu.se.

[†]Assistant Professor, Department of Information Technology, Uppsala University, S-751-05 Uppsala, Sweden, axel.malqvist@it.uu.se

[‡]Research Assistant, Department of Mathematics, Umeå University, S-901-87 Umeå, Sweden, robert.soderlund@math.umu.se.

In this paper we consider a hyperbolic problem with multiscale features in the advection coefficient. We seek the concentration u such that,

$$\dot{u} + \nabla \cdot (\boldsymbol{\sigma}u) = f, \tag{1.1}$$

where $\boldsymbol{\sigma}$ is the multiscale advecting velocity field, and f is a source term. There are numerous applications for this equation e.g. two phase flow in an oil reservoir. The velocity $\boldsymbol{\sigma}$ is there given by Darcy's law.

1.1 Previous work

There has been a lot of work on stabilized finite element methods for solving hyperbolic problems. Streamline diffusion and Galerkin/least-squares are two methods frequently used. Using these techniques standard continuous finite elements, that are unstable for convection dominated problems, can be stabilized by adding an extra term, which depends on the residual of the computed solution, see e.g. [13] and also [8] and references therein. Another popular approach, where this type of excessive stabilization is not needed, is to use discontinuous Galerkin methods, see [10, 12, 4, 7].

A new type of numerical schemes for solving problems with features on several different scales referred to as *multiscale methods* have been introduced over the last fifteen years, see e.g [8, 6]. Here local fine scale problems are solved approximately either using numerical or analytic tools in order to modify a coarse scale problem. The relationship between these methods and the stabilized methods described in the previous paragraph is strong and well presented in [8]. These type of methods have been applied to both pure diffusion and convection dominated problems. In [9] e.g. the variational multiscale method is used to solve a two phase flow problem. The fine scale subgrid problems are there modeled by an algebraic approximation.

In a series of papers [14, 15, 11] authors of the paper have developed an adaptive variational multiscale method (AVMS). In this method the problem is decoupled in a coarse and a fine scale and the fine scale effect on the coarse scale is computed by solving decoupled localized subgrid problems with homogeneous boundary conditions. This method has been applied to elliptic problems on standard and mixed form and for convection dominated problems.

1.2 New contributions

In this paper we apply AVMS to a hyperbolic problem using discontinuous finite element basis functions. Since the flow gives the problem a particular direction we will use directed patches when solving the localized subgrid problems. The direction will depend on the given advection field. This technique reduces the amount of work considerably. We present extensive numerical tests including an example from oil reservoir simulation. We use two spatial dimensions in the numerical examples.

1.3 Outline

In Section 2 we present notations and in Section 3 we present the model problem and the multiscale method. In Section 4 we discuss implementation and in Section 5 numerical examples. Finally we present conclusions in Section 6.

2 Preliminaries

In this section we settle some notations frequently used in the remainder of the paper.

2.1 Function spaces and discretisation

We let $\Omega \subset \mathbf{R}^d$, where $d = 1, 2, 3$, be a domain with polygonal boundary $\partial\Omega$. We let $L^2(\Omega)$ be the set of square integrable functions on Ω . Further we let $H^1(\Omega)$ denote the space of functions that are in $L^2(\Omega)$ and that have gradients in $L^2(\Omega)^d$, and $H(\text{div}, \Omega)$ be the functions in $L^2(\Omega)^d$ which also have divergence in $L^2(\Omega)$. We introduce the standard norms $\|v\|_{L^2(\Omega)} = (\int_{\Omega} v^2 dx)^{1/2}$ and $\|v\|_{H^1(\Omega)} = (\|v\|_{L^2(\Omega)}^2 + \|\nabla v\|_{L^2(\Omega)^d}^2)^{1/2}$. We let $I = (0, T)$ be a time interval and $L^2(I; H^1(\Omega))$ be the space of functions $v : I \rightarrow H^1(\Omega)$ such that $\int_I \|v(\cdot, t)\|_{H^1(\Omega)}^2 dt < \infty$. We note that $L^2(\Omega)$, $H^1(\Omega)$, $H(\text{div}, \Omega)$, and $L^2(I; H^1(\Omega))$ are Hilbert spaces and we introduce the following notation for the inner product in $L^2(\Omega)$, $(v, w)_{\omega} = \int_{\omega} vw dx$. In the case $\omega = \Omega$ we simply write $(v, w) = (v, w)_{\Omega}$. For an extensive overview of these spaces, see [1].

We consider a coarse scale and a fine scale, which both needs to be discretized. We denote the coarse mesh by \mathcal{K}_H and by $H_K = \text{diam}(K)$ we refer to the diameter of the elements in the coarse mesh. The coarse mesh satisfies $\cup_{K \in \mathcal{K}_H} K = \Omega$ where all K are disjoint. The fine mesh however, is only defined on local subregions $\omega \subset \Omega$. The meshes will be nested so that all subregions are unions of coarse elements. We therefore let $\mathcal{K}_H(\omega) = \{K \in \mathcal{K}_H : K \subset \omega\}$, and $\mathcal{K}_h(\omega)$ be the set of fine scale elements $\{K\}$ such that $\cup_{K \in \mathcal{K}_h(\omega)} K = \omega$. Since the meshes are nested all $K \in \mathcal{K}_H(\omega)$ can be written as a union of elements in $\mathcal{K}_h(\omega)$.

We let $\mathcal{V} = L^2(\Omega)$. The corresponding finite element space on the coarse scale will be denoted \mathcal{V}_c and defined in the following way,

$$\mathcal{V}_c = \mathcal{P}_H = \{v : v|_K = \mathcal{P}(K) \quad \forall K \in \mathcal{K}_H\}, \quad (2.1)$$

where $\mathcal{P}(K)$ is the space of linear polynomials on K . We want an hierarchical split between the coarse and the fine spaces. We introduce the $L^2(\Omega)$ -projection $P_H : \mathcal{V} \rightarrow \mathcal{V}_c$, which projects any function in \mathcal{V} onto the coarse finite element space, and define the fine scale space \mathcal{V}_f by

$$\mathcal{V}_f = \{v \in \mathcal{V} : P_H v = 0\}. \quad (2.2)$$

We let $\mathcal{P}_h(\omega)$ be the piecewise linear polynomials on the subgrid $\mathcal{K}_h(\omega)$. The fine scale finite element spaces can now be defined in the following way

$$\mathcal{P}_{h,f}(\omega) = \{v \in \mathcal{P}_h(\omega) : P_H v = 0\}, \quad (2.3)$$

where $\mathcal{P}_{h,f}(\omega)$ approximates \mathcal{V}_f on the subregion ω .

2.2 Jumps and averages

Let us now introduce the set of interior edges \mathcal{E}_I , and boundary edges \mathcal{E}_Γ on the mesh \mathcal{K}_H such that $\mathcal{E}_I \cup \mathcal{E}_\Gamma = \mathcal{E}$. For a function $v \in \mathcal{V}_c$ we define the jump $[v]$ across edge E as

$$[v] = \begin{cases} v^+ - v^-, & E \in \mathcal{E}_I, \\ v^+, & E \in \mathcal{E}_\Gamma, \end{cases} \quad (2.4)$$

where $v^\pm = \lim_{s \rightarrow 0} v(\mathbf{x} \mp s\mathbf{n})$, \mathbf{n} being the edge normal. The average $\langle v \rangle$ is defined by

$$\langle v \rangle = \begin{cases} (v^+ + v^-)/2, & E \in \mathcal{E}_I, \\ v^+, & E \in \mathcal{E}_\Gamma, \end{cases} \quad (2.5)$$

and given a flux velocity $\boldsymbol{\sigma}$, the upwind value \tilde{v} relative that flux velocity, is defined at every edge E , with normal \mathbf{n} as

$$\tilde{v} = \begin{cases} v^+, & \mathbf{n} \cdot \boldsymbol{\sigma} > 0, \\ v^-, & \mathbf{n} \cdot \boldsymbol{\sigma} < 0, \\ \langle v \rangle, & \mathbf{n} \cdot \boldsymbol{\sigma} = 0. \end{cases} \quad (2.6)$$

We use the same notation for edges, jumps, averages, and upwind values for corresponding quantities on the fine scale space \mathcal{V}_f .

2.3 The patches ω_i

Finally we define patches ω_i on which the fine scale finite element spaces are constructed. We let $\text{span}(\{\varphi_i\}_{i \in \mathcal{N}}) = \mathcal{V}_c$ be the standard piecewise linear discontinuous basis functions. This means that $\text{supp}(\varphi_i)$ is exactly one coarse element in the mesh \mathcal{K}_H . Around the support of each basis function φ_i we will construct a patch ω_i of coarse elements on which we will solve localized fine scale problems. In the definition of the patches we will also be referring to the standard piecewise linear continuous functions on the mesh \mathcal{K}_H , which we denote by $\{\theta_i\}$. The patches will include the support of the associated basis function and we will present two different versions, a symmetric version and a directed (with the flow) version.

Definition 2.1. *We say that ω_i^1 is a symmetric 1-layer patch if $\omega_i^1 = \text{supp}(\varphi_i)$, where φ_i is a coarse basis function, with support on one coarse element. Further we define a symmetric k -layer patch, ω_i^k , around the support of basis function φ_i ,*

$$\omega_i^k = \cup_{\{j: \text{supp}(\theta_j) \cap \omega_i^{k-1} \neq \emptyset\}} \text{supp}(\theta_j), \quad k = 2, 3, \dots \quad (2.7)$$

where θ_j is a coarse scale piecewise linear continuous basis function. Furthermore we let $\vec{\omega}_i^k$ be a directed k -layer patch such that $\vec{\omega}_i^1 = \omega_i^1$, $\vec{\omega}_i^k \subset \omega_i^k$ possibly equal, and any $K \in \vec{\omega}_i^k$ can be reached from $\vec{\omega}_i^{k-1}$ by passing from element K^- to element K^+ (starting from any element in $\vec{\omega}_i^{k-1}$) through the shared face F only if $\max_{x \in F} \mathbf{n}^- \cdot \boldsymbol{\sigma}(x) > 0$, where \mathbf{n}^- is the outward normal of K^- . In the text we omit the superscript k .

Examples of these patches are illustrated in Figure 1.

3 Multiscale and dG(1)-method for the time dependent convection equation

We consider the following hyperbolic model problem. For simplicity we assume that all given data is independent of time: find the concentration $u \in L^2(I; H^1(\Omega))$ such that

$$\dot{u} + \nabla \cdot (\boldsymbol{\sigma}u) = f, \quad \text{in } \Omega \times I, \quad (3.1a)$$

$$\mathbf{n} \cdot \nabla u = 0, \quad \text{on } \Gamma_+ \times I, \quad (3.1b)$$

$$u = g, \quad \text{on } \Gamma_- \times I, \quad (3.1c)$$

$$u = u_0, \quad \text{on } \Omega \times \{0\}, \quad (3.1d)$$

where $I = (0, T)$ is the time interval, $f \in L^2(\Omega)$ is a source term, $\boldsymbol{\sigma} \in H(\text{div}; \Omega)$ is the advection field, $g \in H^{1/2}(\Gamma)$ defines the boundary value at the Dirichlet part of the boundary, and $u_0 \in H^1(\Omega)$ is the initial concentration. The segments Γ_+, Γ_- are disjoint parts of the boundary such that $\Gamma_+ \cup \Gamma_- = \Gamma$ and $\Gamma_- = \{x \in \partial\Omega : \mathbf{n} \cdot \boldsymbol{\sigma} < 0\}$, where \mathbf{n} is the outward unit normal of $\partial\Omega$. We usually refer to Γ_- as the inflow part of the boundary. For simplicity we assume that f, g , and $\boldsymbol{\sigma}$ are independent of time.

3.1 The dG(1) method

We let \mathcal{K} be a shape regular mesh of the domain Ω , and further let $\mathcal{V}_h = \{v : v|_K \in \mathcal{P}(K) \ \forall K \in \mathcal{K}\}$. The dG(1) finite element method for (3.1), as described in [3], reads, find $u_h \in \mathcal{V}_h$ such that

$$\begin{aligned} & \sum_{K \in \mathcal{K}} (\dot{u}_h, v)_K - \sum_{K \in \mathcal{K}} (u_h, \boldsymbol{\sigma} \cdot \nabla v)_K + \sum_{E \in \mathcal{E} \setminus \Gamma_-} (\mathbf{n} \cdot \boldsymbol{\sigma} \tilde{u}_h, [v])_E \\ & = (f, v) - \sum_{E \in \Gamma_-} (\mathbf{n} \cdot \boldsymbol{\sigma}, gv)_E, \quad \forall v \in \mathcal{V}_h \ \forall t \in I. \end{aligned} \quad (3.2)$$

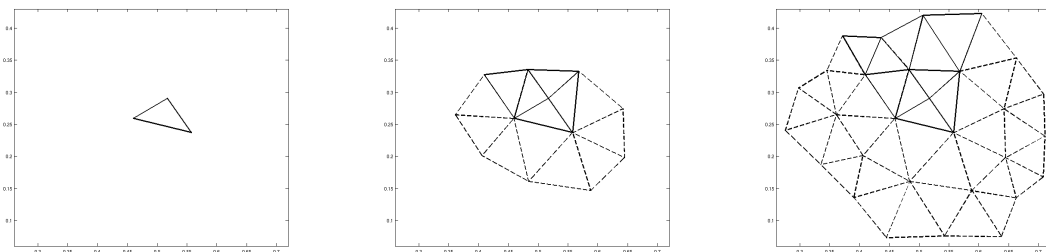


Figure 1: 1, 2, and 3 layer patches of symmetric (dashed) and directed (solid) type. Here $\boldsymbol{\sigma} = [0, 1]$. Note that the directed patches are subsets of the symmetric patches and that they are equal for 1 layer patches.

Using that $\mathbf{n} \cdot \boldsymbol{\sigma} \tilde{u}_h = \mathbf{n} \cdot \boldsymbol{\sigma} \langle u_h \rangle + c_s[u_h]$, where $c_s = |\mathbf{n} \cdot \boldsymbol{\sigma}|/2$, we instead have

$$\begin{aligned} \sum_{K \in \mathcal{K}} (\dot{u}_h, v)_K - \sum_{K \in \mathcal{K}} (u_h, \boldsymbol{\sigma} \cdot \nabla v)_K + \sum_{E \in \mathcal{E}} (\mathbf{n} \cdot \boldsymbol{\sigma} \langle u_h \rangle, [v])_E + \sum_{E \in \mathcal{E}_I} (c_s[u_h], [v])_E \\ = (f, v) - \sum_{E \in \Gamma_-} (\boldsymbol{\sigma} \cdot \mathbf{n}, gv)_E, \quad \forall v \in \mathcal{V}_h, \forall t \in I. \end{aligned} \quad (3.3)$$

If we let

$$q(u, v) = - \sum_{K \in \mathcal{K}} (u, \boldsymbol{\sigma} \cdot \nabla v)_K + \sum_{E \in \mathcal{E}} (\mathbf{n} \cdot \boldsymbol{\sigma} \langle u \rangle, [v])_E + \sum_{E \in \mathcal{E}_I} (c_s[u], [v])_E \quad (3.4a)$$

$$l(v) = (f, v) - \sum_{E \in \Gamma_-} (\boldsymbol{\sigma} \cdot \mathbf{n}, gv)_E, \quad (3.4b)$$

we have

$$(\dot{u}_h, v) + q(u_h, v) = l(v), \quad \forall v \in \mathcal{V}_h, \forall t \in I. \quad (3.5)$$

Let $u^n = u(t_n)$, given u^{n-1} our problem reads

$$(\dot{u}_h, v) + q(u_h, v) = l(v), \quad \forall v \in \mathcal{V}_h, \forall t \in I, \quad (3.6a)$$

$$(u_h(t_{n-1}), v) = (u^{n-1}, v), \quad \forall v \in \mathcal{V}_h. \quad (3.6b)$$

3.2 The variational multiscale formulation

Now we introduce the variational multiscale method for this problem: Find $u = u_c + u_f$, where $u_c \in \mathcal{V}_c$, $u_f \in \mathcal{V}_f$ such that

$$(\dot{u}_c + \dot{u}_f, v_c + v_f) + q(u_c + u_f, v_c + v_f) = l(v_c + v_f), \quad (3.7a)$$

$$\forall v_c \in \mathcal{V}_c, \forall v_f \in \mathcal{V}_f, \forall t \in I,$$

$$(u_c(t_{n-1}) + u_f(t_{n-1}), v_c + v_f) = (u^{n-1}, v_c + v_f), \quad (3.7b)$$

$$\forall v_c \in \mathcal{V}_c, \forall v_f \in \mathcal{V}_f.$$

We split this equation into two parts and use an L^2 -orthogonal split of the coarse and fine scale which cancel the terms (\dot{u}_c, v_f) , and (\dot{u}_f, v_c) . We get

$$(\dot{u}_c, v_c) + q(u_c + u_f, v_c) = l(v_c), \quad \forall v_c \in \mathcal{V}_c, \forall t \in I, \quad (3.8a)$$

$$(u_c(t_{n-1}), v_c) = (u^{n-1}, v_c), \quad \forall v_c \in \mathcal{V}_c, \quad (3.8b)$$

$$(\dot{u}_f, v_f) + q(u_f, v_f) = l(v_f) - q(u_c, v_f), \quad \forall v_f \in \mathcal{V}_f, \forall t \in I, \quad (3.9a)$$

$$(u_f(t_{n-1}), v_f) = (u^{n-1}, v_f), \quad \forall v_f \in \mathcal{V}_f. \quad (3.9b)$$

We use the partition of unities $\{\varphi_i\}_{i \in \mathcal{N}}$ and $\{\chi_i\}_{i \in \mathcal{N}}$, where $\chi_i = \frac{1}{d+1} \text{supp}(\varphi_i)$, and split (3.9) into three parts

$$(\dot{u}_{f,l,i}, v_f) + q(u_{f,l,i}, v_f) = l(\chi_i v_f), \quad \forall v_f \in \mathcal{V}_f, \forall t \in I, \quad (3.10a)$$

$$(u_{f,l,i}(t_{n-1}), v_f) = 0, \quad \forall v_f \in \mathcal{V}_f, \quad (3.10b)$$

$$(\dot{u}_{f,0,i}, v_f) + q(u_{f,0,i}, v_f) = 0, \quad \forall v_f \in \mathcal{V}_f, \forall t \in I, \quad (3.11a)$$

$$(u_{f,0,i}(t_{n-1}), v_f) = (\chi_i u^{n-1}, v_f), \quad \forall v_f \in \mathcal{V}_f, \quad (3.11b)$$

$$(\dot{\mathcal{T}}\varphi_i, v_f) + q(\mathcal{T}\varphi_i, v_f) = -q(\varphi_i, v_f), \quad \forall v_f \in \mathcal{V}_f, \forall t \in I, \quad (3.12a)$$

$$(\mathcal{T}\varphi_i(t_{n-1}), v_f) = 0, \quad \forall v_f \in \mathcal{V}_f. \quad (3.12b)$$

We have thereby used the linearity of the problem to split the fine scale contribution into one part driven by the right hand side functional l , one driven by the solution at the previous time step, and one driven by the coarse scale solution, which is a linear combination coarse basis function φ_i , $u_c = \sum_{i \in \mathcal{N}} \alpha_i \varphi_i$. We note that $u_f = \sum_{i \in \mathcal{N}} (u_{f,l,i} + u_{f,0,i} + \alpha_i \mathcal{T}\varphi_i)$. Using these quantities the coarse scale equation (3.8) now reads

$$(\dot{u}_c, v_c) + q(u_c + \mathcal{T}u_c, v_c) = l(v_c) - q(u_{f,l} + u_{f,0}, v_c), \quad \forall v_c \in \mathcal{V}_c, \forall t \in I, \quad (3.13a)$$

$$(u_c(t_{n-1}), v_c) = (u^{n-1}, v_c), \quad \forall v_c \in \mathcal{V}_c, \quad (3.13b)$$

where $\mathcal{T}u_c = \sum_{i \in \mathcal{N}} \alpha_i \mathcal{T}\varphi_i$, $u_{f,l} = \sum_{i \in \mathcal{N}} u_{f,l,i}$, and $u_{f,0} = \sum_{i \in \mathcal{N}} u_{f,0,i}$.

3.3 Spatial discretization of fine scale equations

We will now use the discrete function spaces on patches to formulate an approximate method. We keep the continuous formulation in time for now. We let $U_{f,l,i}(t), U_{f,0,i}(t), \mathcal{T}\varphi_i(t) \in \mathcal{P}_{h,f}(\omega_i)$ solve,

$$(\dot{U}_{f,l,i}, v_f) + q(U_{f,l,i}, v_f) = l(\chi_i v_f), \quad \forall v_f \in \mathcal{P}_{h,f}(\omega_i), \forall t \in I, \quad (3.14a)$$

$$(U_{f,l,i}(t_{n-1}), v_f) = 0, \quad \forall v_f \in \mathcal{P}_{h,f}(\omega_i), \quad (3.14b)$$

$$(\dot{U}_{f,0,i}, v_f) + q(U_{f,0,i}, v_f) = 0, \quad \forall v_f \in \mathcal{P}_{h,f}(\omega_i), \forall t \in I, \quad (3.15a)$$

$$(U_{f,0,i}(t_{n-1}), v_f) = (\chi_i U^{n-1}, v_f), \quad \forall v_f \in \mathcal{P}_{h,f}(\omega_i), \quad (3.15b)$$

$$((\dot{\mathcal{T}}\varphi_i), v_f) + q(\mathcal{T}\varphi_i, v_f) = -q(\varphi_i, v_f), \quad \forall v_f \in \mathcal{P}_{h,f}(\omega_i), \forall t \in I, \quad (3.16a)$$

$$(\mathcal{T}\varphi_i(t_{n-1}), v_f) = 0, \quad \forall v_f \in \mathcal{P}_{h,f}(\omega_i), \quad (3.16b)$$

for all $i \in \mathcal{N}$.

Remark 3.1 The inflow boundary segments Γ_-^i of the local problem on ω_i will have homogeneous Dirichlet boundary conditions and the rest of the boundary $\partial\omega_i \setminus \Gamma_-^i$ will have homogeneous Neumann boundary conditions. We interpret the functions in $\mathcal{P}_{h,f}(\omega_i)$ to be zero outside ω_i in order to use the same definition for q and l also for the local problems.

3.4 Spatial discretization of the coarse scale equation

If $U_c = \sum_{i \in \mathcal{N}} \alpha_i \varphi_i$, then $U_f = \sum_{i \in \mathcal{N}} (U_{f,l,i} + U_{f,0,i} + \alpha_i T \varphi_i)$ and we get the following for the coarse scale equation (3.8)

$$(\dot{U}_c, v_c) + q(U_c + T U_c, v_c) = l(v_c) - q(U_{f,l} + U_{f,0}, v_c), \quad \forall v_c \in \mathcal{V}_c, \forall t \in I, \quad (3.17a)$$

$$(U_c(t_{n-1}), v_c) = (U^{n-1}, v_c), \quad \forall v_c \in \mathcal{V}_c, \quad (3.17b)$$

where $U_{f,l} = \sum_{i \in \mathcal{N}} U_{f,l,i}$ and $U_{f,0} = \sum_{i \in \mathcal{N}} U_{f,0,i}$.

3.5 Discretization in time

We let $0 = t_0 < t_1 < \dots < t_L = T$ and $dt = t_n - t_{n-1}$ for all $n = 1, 2, \dots, L$. Using the Crank-Nicholson time stepping scheme the fine scale equations (3.14)-(3.16) reads: given $U_{f,l,i}^{n-1}, U_{f,0,i}^{n-1}, T \varphi_i^{n-1}, \alpha_i^{n-1}$ find $U_{f,l,i}^n, U_{f,0,i}^n, T \varphi_i^n$ such that (using that $T \varphi_i^{n-1} = U_{f,l,i}^{n-1} = 0$)

$$(\dot{U}_{f,l,i}, v_f) + \frac{1}{2} q(U_{f,l,i}^n, v_f) = l(\chi_i v_f) - \frac{\alpha_i^{n-1}}{2} q(\varphi_i, v_f), \quad \forall v_f \in \mathcal{P}_{h,f}(\omega_i), \quad (3.18a)$$

$$(U_{f,l,i}(t_{n-1}), v_f) = 0, \quad \forall v_f \in \mathcal{P}_{h,f}(\omega_i), \quad (3.18b)$$

$$(\dot{U}_{f,0,i}, v_f) + \frac{1}{2} q(U_{f,0,i}^n, v_f) = -\frac{1}{2} q(U_{f,0,i}^{n-1}, v_f), \quad \forall v_f \in \mathcal{P}_{h,f}(\omega_i), \quad (3.19a)$$

$$(U_{f,0,i}(t_{n-1}), v_f) = (\chi_i U^{n-1}, v_f), \quad \forall v_f \in \mathcal{P}_{h,f}(\omega_i), \quad (3.19b)$$

$$((T \varphi_i), v_f) + \frac{1}{2} q(T \varphi_i^n, v_f) = -\frac{1}{2} q(\varphi_i, v_f), \quad \forall v_f \in \mathcal{P}_{h,f}(\omega_i), \quad (3.20a)$$

$$(T \varphi_i(t_{n-1}), v_f) = 0, \quad \forall v_f \in \mathcal{P}_{h,f}(\omega_i). \quad (3.20b)$$

We note that $\sum_{i \in \mathcal{N}} \alpha_i^n T \varphi_i + U_{f,l,i}^n + U_{f,0,i}^n = U_f^n$ by linearity. The modified coarse scale equation (3.17) reads: given $U_{f,l,0}^n, U_{f,l,0}^{n-1}, T U_c, U_c^{n-1}$, find U_c^n , such that

$$(\dot{U}_c, v_c) + \frac{1}{2} q((I + T) U_c^n, v_c) = \quad (3.21a)$$

$$= l(v_c) - \frac{1}{2} q((I + T) U_c^{n-1} + U_{f,l}^n + U_{f,l}^{n-1} + U_{f,0}^n + U_{f,0}^{n-1}, v_c),$$

$$(U_c(t_{n-1}), v_c) = (U^{n-1}, v_c), \quad (3.21b)$$

for all $v_c \in \mathcal{V}_c$.

Remark 3.2 In this work we assume the same time step on the coarse and fine scale. A natural extension will be to allow different time steps. Equations (3.18,3.19,3.20) will then be solved on each coarse time interval $[t_{n-1}, t_n]$ using many (fine) time steps.

4 Implementation

We now have three very similar systems of fine scale equations and a coarse scale equation that need to be solved. We describe how to treat the third fine scale equation and the coarse scale equation in detail. The other two fine scale equations will be handled in a very similar way.

4.1 The fine scale equations

We let \mathcal{E}_I^i be the set of all interior edges and \mathcal{E}_Γ^i be the set of all boundary edges in the mesh $\mathcal{K}_h(\omega_i)$. Furthermore we let Γ_-^i be the inflow part of the boundary $\partial\omega_i$. We introduce the following matrix and vector notations,

$$M_{jk}^i = (\varphi_k, \varphi_j)_{\omega_i}, \quad (4.1a)$$

$$Q_{jk}^i = (\mathbf{n} \cdot \boldsymbol{\sigma} \langle \varphi_k \rangle, [\varphi_j])_{\mathcal{E}_\Gamma^i \setminus \Gamma_-^i} + (c_s[\varphi_k], [\varphi_j])_{\mathcal{E}_I^i}, \quad (4.1b)$$

$$K_{jk}^i = -(\varphi_k, \boldsymbol{\sigma} \cdot \nabla \varphi_j)_{\omega_i}, \quad (4.1c)$$

$$b_j^i = (\chi_i f, \varphi_j)_{\omega_i} - (\mathbf{n} \cdot \boldsymbol{\sigma}, g \varphi_j)_{\mathcal{E}_\Gamma^i \cap \Gamma_-^i}. \quad (4.1d)$$

We consider equation (3.20) which gives us the following matrix equation

$$(M^i + \frac{dt}{2}(K^i + Q^i + R^i))T\vec{\varphi}_i^n = \frac{1}{2}(K^i + Q^i + R^i)\vec{\varphi}_i, \quad \mathcal{P}_H T\vec{\varphi}_i^n = 0, \quad (4.2)$$

where $T\vec{\varphi}_i$, $\vec{\varphi}_i$ are the vectors of nodal values of $T\varphi_i$, φ_i and \mathcal{P}_H is the matrix corresponding to the L^2 projection operator P_H . The additional condition $\mathcal{P}_H T\vec{\varphi}_i = 0$ is realized using Lagrange multipliers.

Remark 4.1 Since $\boldsymbol{\sigma}$ and f are time independent, $T\vec{\varphi}_i$ does not vary in time. Furthermore, since we have orthogonality of the coarse and fine scales in L^2 the only data which varies between the time steps when computing $\vec{U}_{f,l,i}^n$, and $\vec{U}_{f,0,i}^n$ for different n are $\vec{U}_{f,0,i}^{n-1}$, and α_i^{n-1} . This means that we need to compute and store these quantities and also that we need some minor communication between neighboring patches in order to compute $\chi_i \vec{U}_{f,0}^{n-1}$.

4.2 The coarse scale equations

Again we discretize in time and use equations (3.14-3.16) to get the fine scale contribution. Let $0 = t_0 < t_1 < \dots < t_L = T$ and $dt = t_n - t_{n-1}$ for all $n = 1, 2, \dots, L$. We use

the Crank-Nicholson time stepping scheme, given \vec{U}_c^{n-1} , to compute \vec{U}_c^n by solving the following matrix equation

$$(M + \frac{dt}{2}(K + Q + R))\vec{U}_c^n = (M - \frac{dt}{2}(K + Q + R))\vec{U}_c^{n-1} + dt(b - r), \quad (4.3)$$

where \vec{U}_c is the vector of nodal values of U_c and,

$$M_{jk} = (\varphi_k, \varphi_j), \quad (4.4a)$$

$$Q_{jk} = (n \cdot \sigma \langle \varphi_k \rangle, [\varphi_j])_{\mathcal{E}_\Gamma \setminus \Gamma_-} + (c_s [\varphi_k], [\varphi_j])_{\mathcal{E}_I}, \quad (4.4b)$$

$$R_{jk} = (n \cdot \sigma \langle T\phi_k \rangle, [\varphi_j])_{\mathcal{E}_\Gamma \setminus \Gamma_-} + (c_s [T\phi_k], [\varphi_j])_{\mathcal{E}_I}, \quad (4.4c)$$

$$K_{jk} = -(\varphi_k, \sigma \cdot \nabla \varphi_j), \quad (4.4d)$$

$$b_j = (f, \varphi_j) - (\sigma \cdot n, g\varphi_j)_{\mathcal{E}_\Gamma \cap \Gamma_-}, \quad (4.4e)$$

$$r_j = (n \cdot \sigma \langle u_{f,l,0}^n + u_{f,l,0}^{n-1} \rangle, [\varphi_j])_{\mathcal{E}_\Gamma \setminus \Gamma_-} + (c_s [u_{f,l,0}^n + u_{f,l,0}^{n-1}], [\varphi_j])_{\mathcal{E}_I}. \quad (4.4f)$$

The method for solving the equation (3.1) is to first solve (3.10)-(3.12) and then (4.3) and repeat this for all time steps. Note that if the patches $\omega_i = \Omega$ and the same resolution is used in all patches the reference solution on the fine mesh is recovered. This is not a realistic technique in practise but it indicates that a solution on the fine scale mesh will serve as a good reference solution when studying how the truncated domains ω_i affects the approximate solution $U_c + U_f$. The difference between the reference solution and $U_c + U_f$ will be studied in the numerical examples below.

4.3 Numerical algorithm

We end this Section with a numerical algorithm for the entire method. We can use the same patches ω_i for all time steps. This will of course increase the speed and efficiency of the method.

Algorithm 1

- 1: Assemble the local fine scale matrices M^i , K^i , Q^i , and vector b^i on each patch and the global matrices M , K , Q , and vector b .
 - 2: Compute the time independent fine scale solution $T\vec{\varphi}_i$, for all $i \in \mathcal{N}$ and assemble the global matrix R .
 - 3: **for** $n = 1, \dots, L$ **do**
 - 4: Loop over all elements $i \in \mathcal{N}$ and compute $\vec{U}_{f,0,i}^n$, $\vec{U}_{f,l,i}^n$ given $\vec{U}_{f,0,i}^{n-1}$, $\vec{U}_{f,l,i}^{n-1}$, \vec{U}_c^{n-1} and $T\vec{\varphi}_i$.
 - 5: **end for**
 - 6: Assemble the right hand side r in equation (4.4f).
 - 7: Compute \vec{U}_c^n by solving equation (4.3).
 - 8: *Optional*: Construct $U = U_c + U_f$ using \vec{U}_c , and $\vec{U}_{f,0,i}$, $\vec{U}_{f,l,i}$, $T\vec{\varphi}_i$ for all $i \in \mathcal{N}$.
-

5 Numerical examples

We will consider two different problems in the numerical section. The first is a test case defined in the following way,

$$\text{(Case 1)} \quad \Omega = [0, 1] \times [0, 1], \quad \Gamma_- = [0, 1] \times \{0\}, \quad \boldsymbol{\sigma} = [0, 1], \quad g = 0, \quad f = 1.$$

The second test case has a more realistic advection field. We let $\boldsymbol{\sigma}$ be the velocity field solving the pressure equation, find the pressure p and the advection field $\boldsymbol{\sigma}$ such that

$$-\nabla \cdot \boldsymbol{\sigma} = F, \quad \text{in } \Omega, \quad (5.1a)$$

$$\boldsymbol{\sigma} = a \nabla p, \quad \text{in } \Omega, \quad (5.1b)$$

$$\boldsymbol{n} \cdot \boldsymbol{\sigma} = 0, \quad \text{on } \partial\Omega, \quad (5.1c)$$

where F is a given source term equal to one in the lower left corner (injector) and minus one in the upper right corner (producer), and a is the permeability, taken from the top layer of the SPE tenth comparative solution project, see <http://www.spe.org/web/csp/>. Given $\boldsymbol{\sigma}$ from equation (5.1) (see Figure 2) we let,

$$\text{(Case 2)} \quad \Omega = [0, 1] \times [0, 1], \quad \boldsymbol{\sigma} \text{ from (5.1)}, \quad f = \chi_{\text{inj}} - \chi_{\text{prod}} u.$$

where χ_{inj} , χ_{prod} are the characteristic functions of the injector and the producer respectively. Note that due to (5.1c) we have no inflow boundary in this example and the flow is driven by a source term similar to F in (5.1a). The term $-\chi_{\text{prod}} u$ makes sure that u reaches a stationary value at the producer, instead of growing without bound.

We will measure error in the broken $H^1(\Omega)$ -norm which we denote by $\|\cdot\|$ and define as

$$\|\|v\|\| = \sum_{K \in \mathcal{K}} \|v\|_{H^1(K)}. \quad (5.2)$$

For the second case we will also consider the break through time. This is when the concentration at the producer is close to one (we pick 0.95), i.e. the time t^* , such that the concentration of water in the producing spot is 95%, $u(\text{prod}, t^*) = 0.95$.

5.1 Convergence of local solutions

We focus on equation (4.3) which is solved to compute $U_{f,l,i}$ at the next time step. The other two types of fine scale equations show very similar behavior. We first consider both cases 1 and 2 and fix $dt = 0.005$ for case 1 and $dt = 1$ for case 2. The reason for the large difference in the time steps chosen is due to the difference in the magnitude of the convective fields. For both examples the fine scale is obtained from uniformly dividing each coarse triangle into 16 smaller triangles.

The patch sizes are varied using the two different patch types described in Definition 2.1. We plot the convergence in broken H^1 -norm compared with a reference solution. The relative error is plotted against degrees of freedoms of the local problems.

As our coarse scale meshes, we use the meshes depicted in Figure 3. We will consider convergence of $T\varphi_{216}$ for case 1 and convergence of $T\varphi_{210}$ for case 2. Those fine scale functions corresponds to one of the basis functions in the black triangles in Figure 3. The solutions for $T\varphi_{216}$ and $T\varphi_{210}$ are found in Figure 4-5. Convergence plots for $T\varphi_{216}$ and $T\varphi_{210}$ are found in Figure 6. We compare with $T\varphi_{216}$ and $T\varphi_{210}$ computed on the whole domain Ω and plot the relative error in broken H^1 -norm against the degrees of freedoms of the local problems. We can observe an exponential convergence for directed patches of the error of the local problems and we also note the advantages with the directed type (b) patches that clearly yields a faster rate of convergence. In Figure 7 we have the corresponding convergence plots but with time steps $dt = 0.05$ and $dt = 10$. Obviously the rate of convergence is greatly affected by the time step, which is natural since the local solutions will be transported further and thus larger patches are needed.

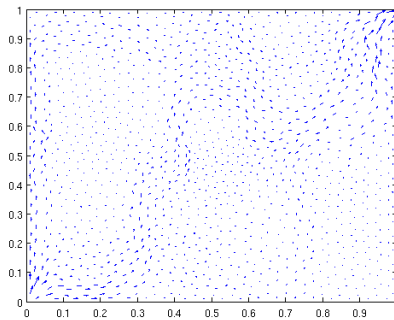


Figure 2: The convective field, σ , used in case 2.

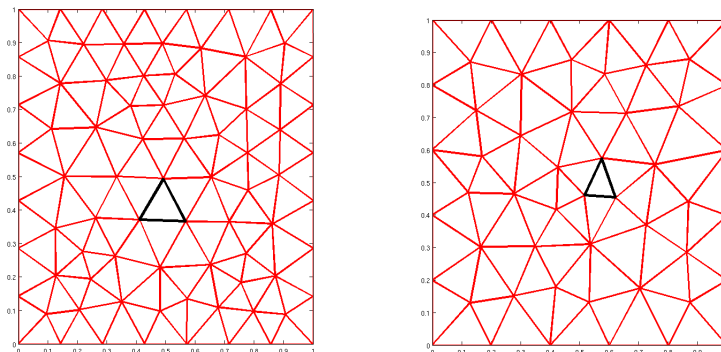


Figure 3: The coarse scale mesh for case 1 (to the left) and the coarse scale mesh for case 2 (to the right). The patches when studying the convergence of $T\varphi_{216}$ and $T\varphi_{210}$ will be constructed around the black triangles.

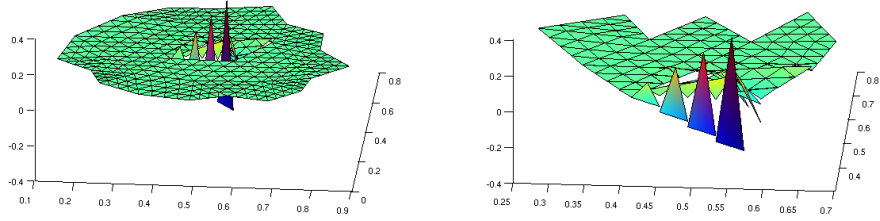


Figure 4: $T\varphi_{216}$ for case 1 with $dt=0.005$, computed on a symmetric type patch (left) and the directed type patch (right).

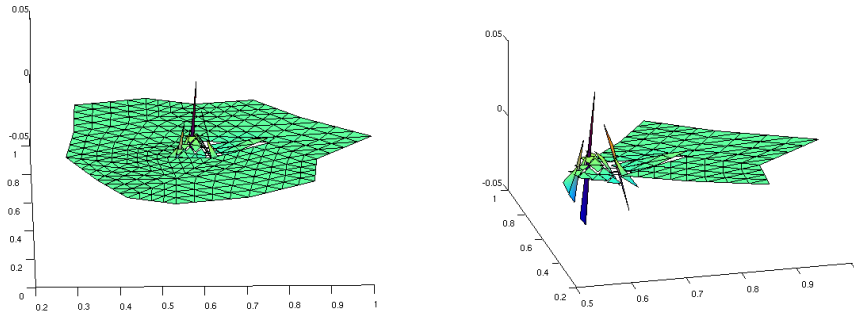


Figure 5: $T\varphi_{210}$ for case 2 with $dt=1$, computed on a symmetric type patch (left) and the directed type patch (right).

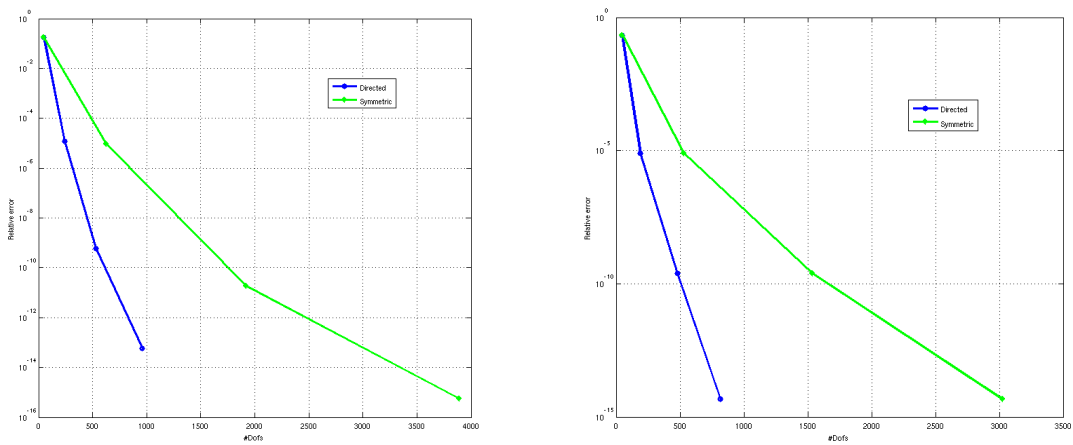


Figure 6: Convergence in broken H^1 -norm of $T\varphi_{216}$ (left) and $T\varphi_{210}$ (right), for the two types of patches with $dt = 0.005$ (left) and $dt = 1$ (right).

Layers	2	3	4
Time steps	1736	1265	1264

Table 1: The number of time steps required to reach the concentration 0.95 at the producer. The reference value is 1264 time steps.

5.2 Convergence of global solution

We are now ready to consider the error in the global solution $U_c + U_f$. We again consider both cases 1 and 2. We consider convergence in broken H^1 -norm and for case 2 also in breakthrough time. We only compute the relative error and breakthrough time using patches having two or more layers. Reference solutions for case 1 and 2 are shown in Figure 8-9. Convergence plots when comparing the error in broken H^1 -norm between the multiscale solutions and the reference solutions are found in Figure 10-11, where the relative error is plotted against the average number of degrees of freedom for the local problems. We can clearly observe the exponential decrease also for the convergence of the global solutions and it is still clear that the directed type patches are considerably more efficient than the symmetric type patches.

For case 2 and the directed patches we also have results for convergence in break through time, here defined as when the concentration at the producer has reached the value 0.95. We have compared the number of time steps required to reach that value and the results are found in Table 1.

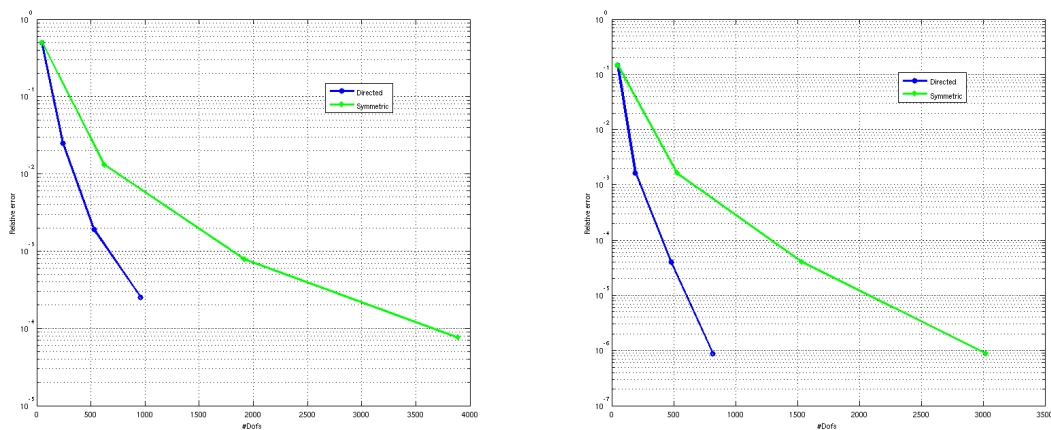


Figure 7: Convergence in broken H^1 -norm of $T\varphi_{216}$ (left) and $T\varphi_{210}$ (right), for the two types of patches with $dt = 0.05$ (left) and $dt = 10$ (right).

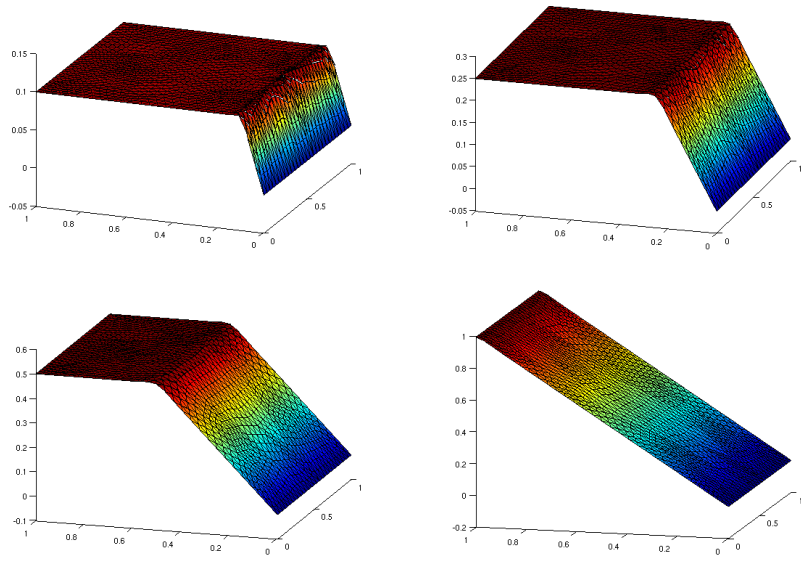


Figure 8: Reference solution for case 1 after 20, 50, 100, and 200 time steps.

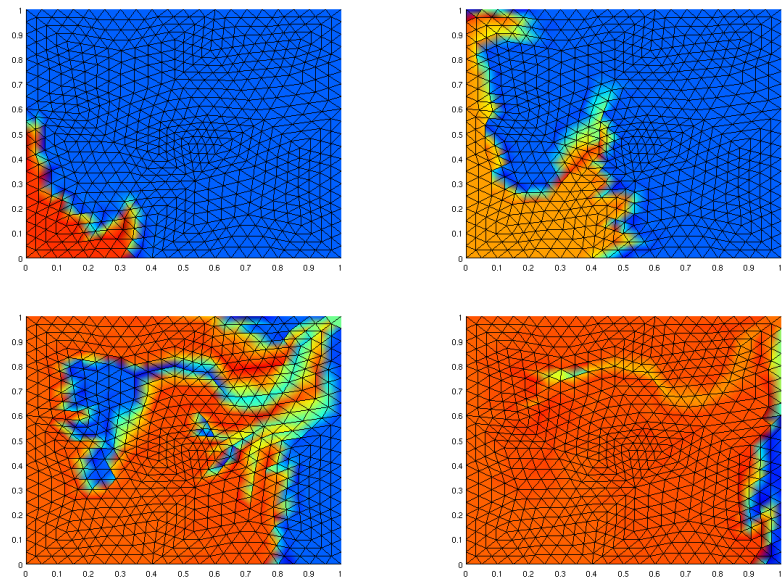


Figure 9: Reference solution for case 2 after 50, 150, 500, and 1500 time steps.

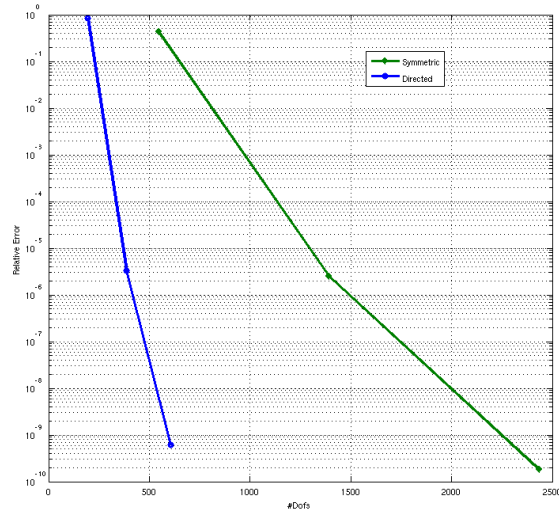


Figure 10: Convergence of relative error in broken H^1 -norm against the average number of degrees of freedoms of the local problems, for the two types of patches in case 1, after 200 time steps.

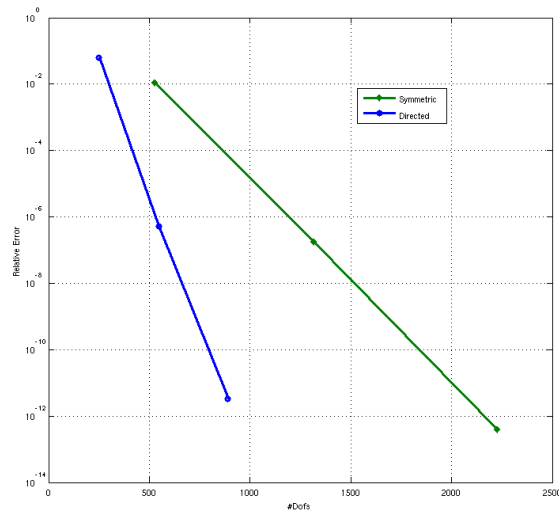


Figure 11: Convergence of relative error in broken H^1 -norm against the average number of degrees of freedoms of the local problems, for the two types of patches in case 2, after 1400 time steps.

6 Conclusions

The exponential decrease in relative error as the patch size increases is a very promising result since it allows for solving the fine scale problems locally and thus making the decoupling more effective.

Since the same patches are used for all time steps and $T\varphi_i$ is time independent, the method can be made very effective. For each time step we only need to compute $U_{f,t,i}$, $U_{f,0,i}$, modify the coarse scale equation and then solve for U_c .

The method can be made even more effective by choosing suitable shapes of the patches and for the hyperbolic equation (3.1), studied in this paper the directed type patches are clearly more efficient than the symmetric type patches.

Further developments of the method includes: using different time steps on the coarse and the fine scale; studying the problem where (5.1) and (3.1) are coupled together; using adaptive variational multiscale methods (AVMS), allowing for different resolution, patch size, and time steps of the local problems; and studying what might be optimal patches for a convection-diffusion equation.

References

- [1] R. A. Adams, *Sobolev Spaces*, Academic Press, San Diego, CA, 1978.
- [2] P. Bochevi, T. J.R. Hughes, and G. Scovazzi, *A Multiscale Discontinuous Galerkin Method*, Lecture Notes in Computer Science, 2006, Volume 3743/2006, 84–93.
- [3] F. Brezzi, L. D. Marini, and E. Süli, *Discontinuous Galerkin methods for first-order hyperbolic problems*, NA-04/02, Oxford University Computing Laboratory, 2004.
- [4] B. Cockburn and C.-W. Shu, *The local discontinuous Galerkin method for time-dependent reaction-diffusion systems*, SIAM J. Numer. Anal., 35 (1998), 2440–2463.
- [5] Y. Efendiev and L. J. Durlofsky, *Numerical modeling of subgrid heterogeneity in two phase flow simulations*, Water Resources Research, Vol. 38, No. 8, (2002).
- [6] Y. R. Efendiev, T. Y. Hou, and X. H. Wu, *Convergence of a nonconforming multiscale finite element method*, SIAM J. Num. Anal., 37 (2000), pp. 888–910.
- [7] P. Houston, C. Schwab, and E. Süli, *Discontinuous hp-finite element methods for advection-diffusion-reaction problems*, SIAM J. Numer. Anal., Vol. 39, No. 6, (2002), 2133–2163.
- [8] T. J. R. Hughes, *Multiscale phenomena: Green’s functions, the Dirichlet-to-Neumann formulation, subgrid scale models, bubbles and the origins of stabilized methods*, Comput. Methods Appl. Mech. Engrg. 127, (1995), 387–401.

- [9] R. Juanes, *A variational multiscale finite element method for multiphase flow in porous media*, *Finite Elements in Analysis and Design*, 41, (2005), 763-777.
- [10] C. Johnson, U. Nävert, and J. Pitkäranta, *Finite element methods for linear hyperbolic problems*, *Comput. Methods Appl. Mech. Engrg.*, 45 (1984), 285-312.
- [11] M. G. Larson and A. Målqvist, *Adaptive variational multiscale method of convection-diffusion problems*, *Comm. Num. Methods Engrg.*, 25, (2009), 65–79.
- [12] C. Johnson and J. Pitkäranta, *An analysis of the discontinuous Galerkin method for a scalar hyperbolic equation*, *Math. Comp.*, 46 (1986), 1-26.
- [13] C. Johnson, A. H. Schatz, and L. B. Wahlbin, *Crosswind smear and pointwise errors in streamline diffusion finite element methods*, *Math. Comp.*, 49, (1987), 25-38.
- [14] M. G. Larson and A. Målqvist, *Adaptive variational multiscale methods based on a posteriori error estimation: Energy norm estimates for elliptic problems*, *Comput. Methods Appl. Mech. Engrg.* 196 (2007) 2313-2324.
- [15] M. G. Larson and A. Målqvist, *A mixed adaptive variational multiscale method with applications in oil reservoir simulation*, *Math. Models Methods Appl. Sci.* 19, (2009), 1017–1042